Supporting Information: Effect of salt on the lamellar L_α-to-MLV transformation in SDS/octanol/water under microfluidic flow

Liva Donina, Lionel Porcar, and João T. Cabral*

July 6, 2022

1 Optical birefringence estimates of the phase boundaries of the SDS/octanol/brine system with varying NaCl content.

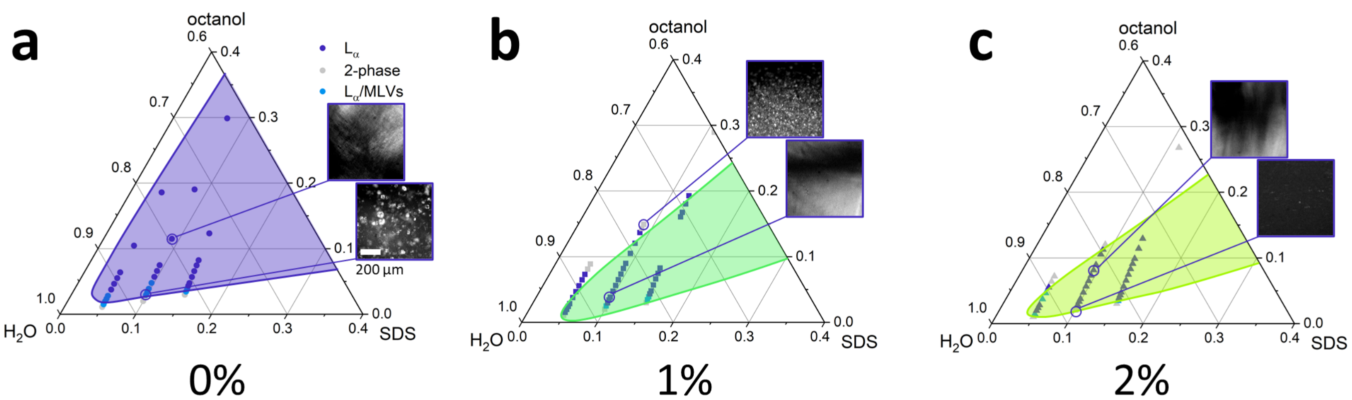

Figure S1: **Phase maps of SDS/octanol/water system with different salt concentrations.** a) 0% NaCl; b) 1% NaCl; c) 2% NaCl.

2 Viscosity measurements for SDS/octanol/brine with varying NaCl content.

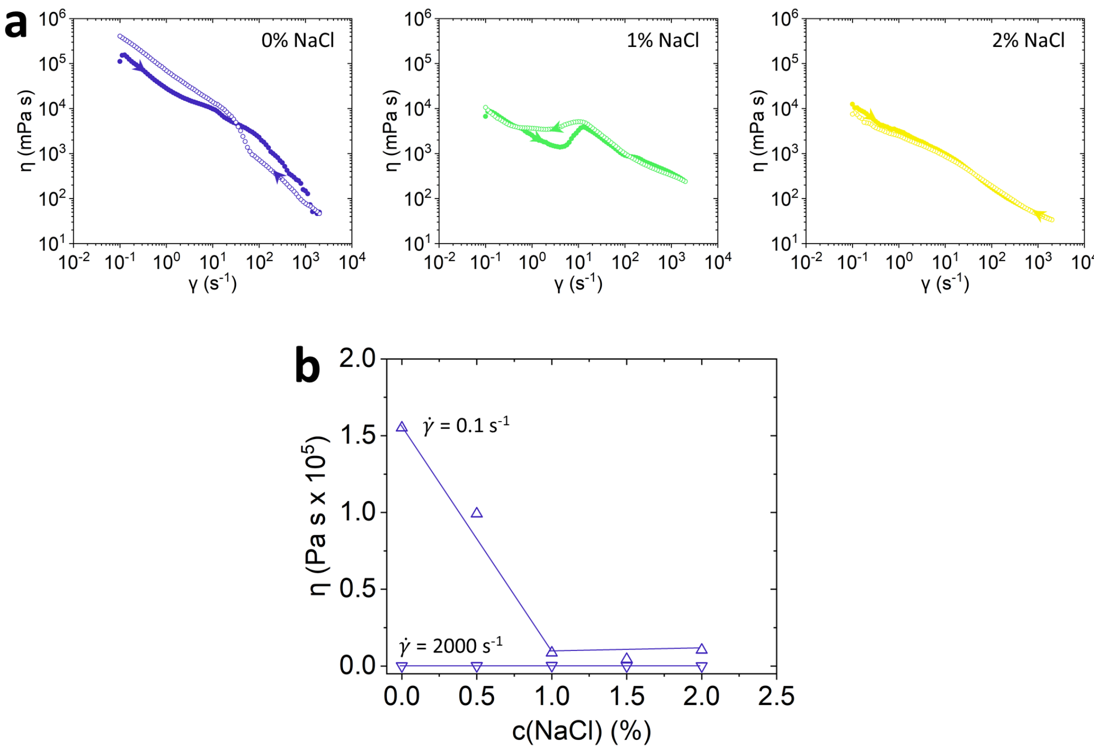

Figure S2: **Rheological characterisation of SDS/octanol/water system with different salt concentrations.** a) Rheological shear sweeps from 0.1 to 2000 s^{-1} for selected salt concentrations for 0%, 1% and 2% NaCl; b)Viscosity η dependence on NaCl concentrations.

3 Microfluidic experimental design, PIV and pressure drop estimates.

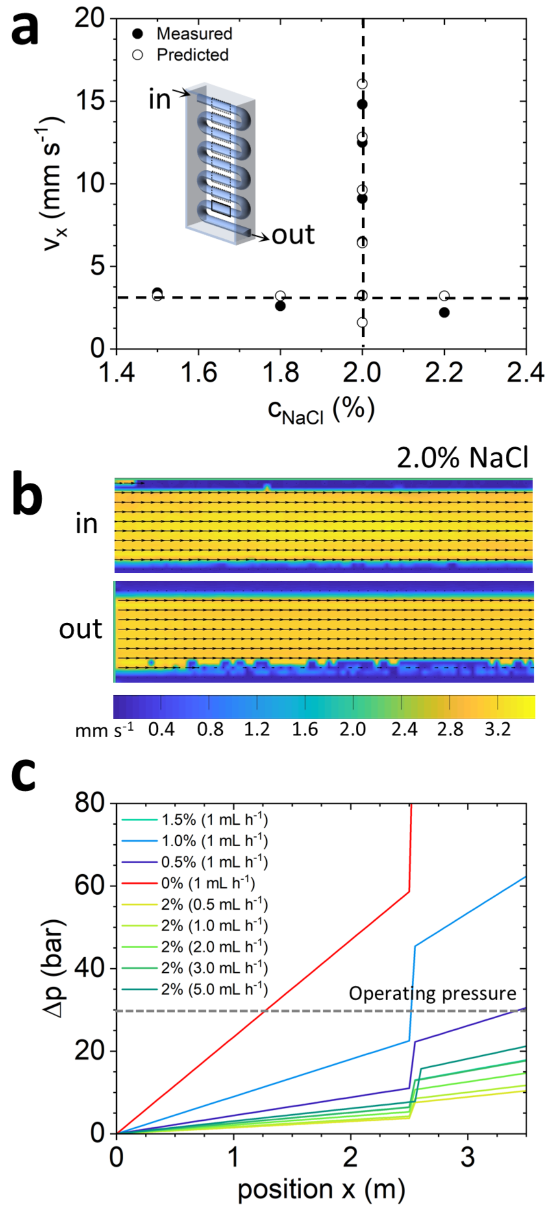

Figure S3: **Overview of flow conditions.** a) Imposed vs measured flow rate v_x; b) PIV of 2.0% NaCl condition at the start and end of the chip showing plug-like flow profile. PIVs were obtained using PIVLab software inputting 20 consecutive images and ensemble correlation with 2 passes with 64x64 and 32x32 pixel by pixel interrogation window sizes (1 pixel = 1.54 μm), and selecting a Gauss 2x3-point sub-pixel estimator and 'standard' correlation quality; c) Pressure drop calculations along the microfluidic chip for various flow and NaCl conditions estimated using Hagen–Poiseuille equation. A maximum safe operating pressure for this microfluidic system is estimated to be 30 bar.

4 SANS contrasts, tabulated fitted values, parameter sensitivity, and compressibility modulus estimates.

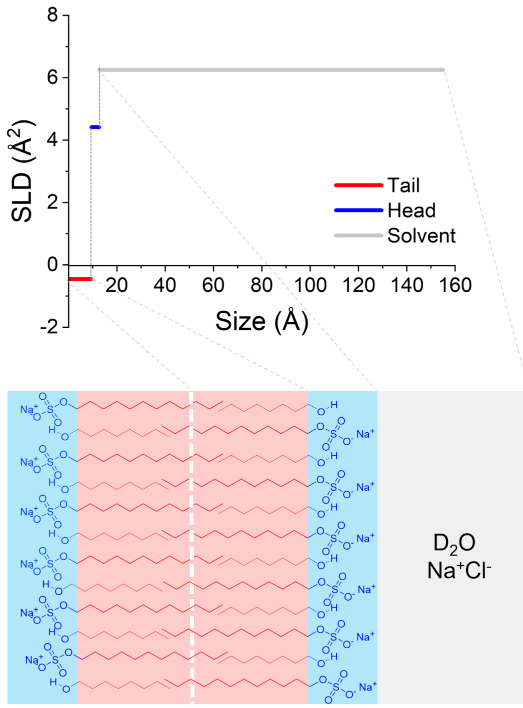

Figure S4: **Scattering length density (SLD) estimates and schematic of the bilayer cross-section.**

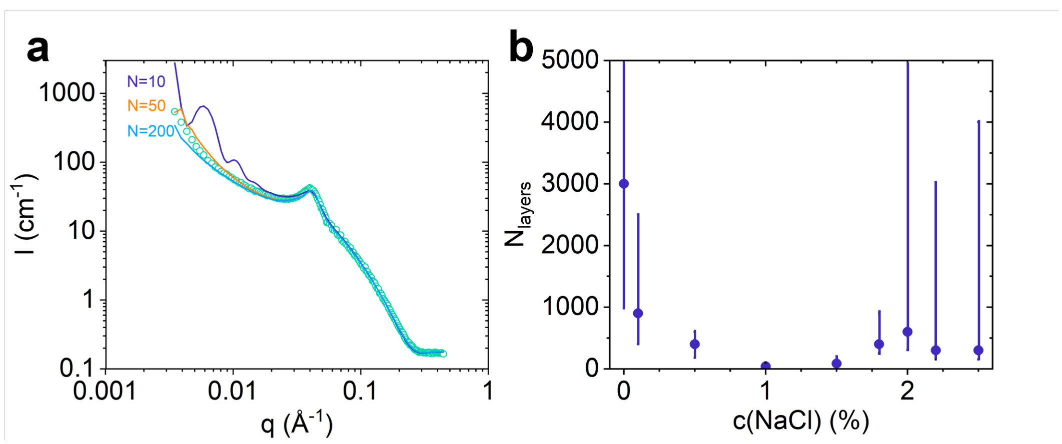

Figure S5: **Model estimate for number of layers** a) Model fit with varying number of L_α layers N=10, 50, 200 for 1.5% NaCl; b) Estimated number of layers N for varying NaCl concentrations

c(NaCl) %	scale	I(incoh) cm^{-1}	l(tail) Å	l(head) Å	δ Å	N layers	d Å	η	SLD (tail) $10^{-6}/Å^2$	SLD (head) $10^{-6}/Å^2$	SLD (solvent) $10^{-6}/Å^2$	polydis	χ^2
0	0.9	0.17	9.4	3.2	25.2	980-10000	156	0.11039	-0.46	4.41	6	0	359
0.1	0.9	0.18	9.4	3.2	24.8	400-2500	156	0.23816	-0.46	4.41	6	0	168
0.5	0.9	0.18	9.4	3.2	24.0	180-600	144	0.77126	-0.46	4.41	6	0	74
1	0.6	0.16	9.4	3.2	26.0	37-100	135	0.99991	-0.46	4.41	6	0.07	370
1.5	0.63	0.17	9.4	3.2	25.5	50-200	147	0.99997	-0.46	4.41	6	0.06	22
1.8	0.7	0.16	9.4	3.2	24.7	250-900	150	0.9999	-0.46	4.41	6	0.08	18
2	0.7	0.16	9.4	3.2	25.0	200-600	156	0.99995	-0.46	4.41	5.8	0.08	57
2.2	0.7	0.17	9.4	3.2	24.9	150-3000	152	0.99996	-0.46	4.41	5.9	0.1	45
2.5	0.5	0.17	9.4	3.2	27.3	150-3000	149	0.9999	-0.46	4.41	6	0.09	63

Figure S6: **Fitted SANS parameters corresponding to Figs. 4 and 5 of the main paper.**

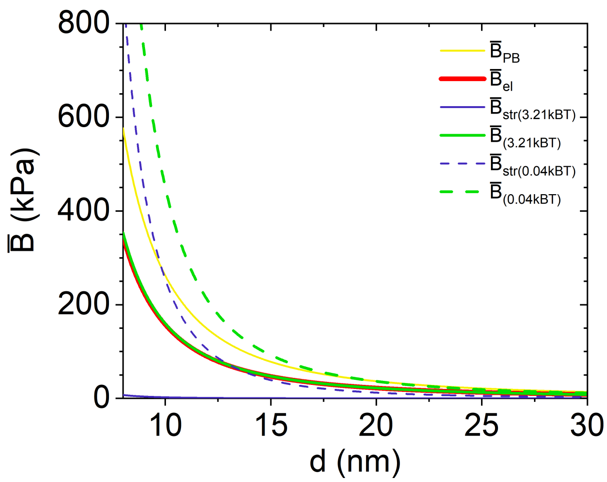

Figure S7: **Membrane compressibility modulus $\overline{B}$ dependence on d-spacing d**. $\overline{B}_{el}$ (red solid line), value adjusted when accounting for spatial correlation of counterions adjacent to membrane and $\overline{B}_{str}$ are summed to obtain $\overline{B}$ values for low and high membrane bending rigidity conditions shown in dashed and solid green colours respectively. $\overline{B}_{PB}$ is the value of membrane compressibility modulus only considering electrostatic contributions without counterion interactions.

5 Extended dataset for SANS results for 2% NaCl under varying flow rate conditions.

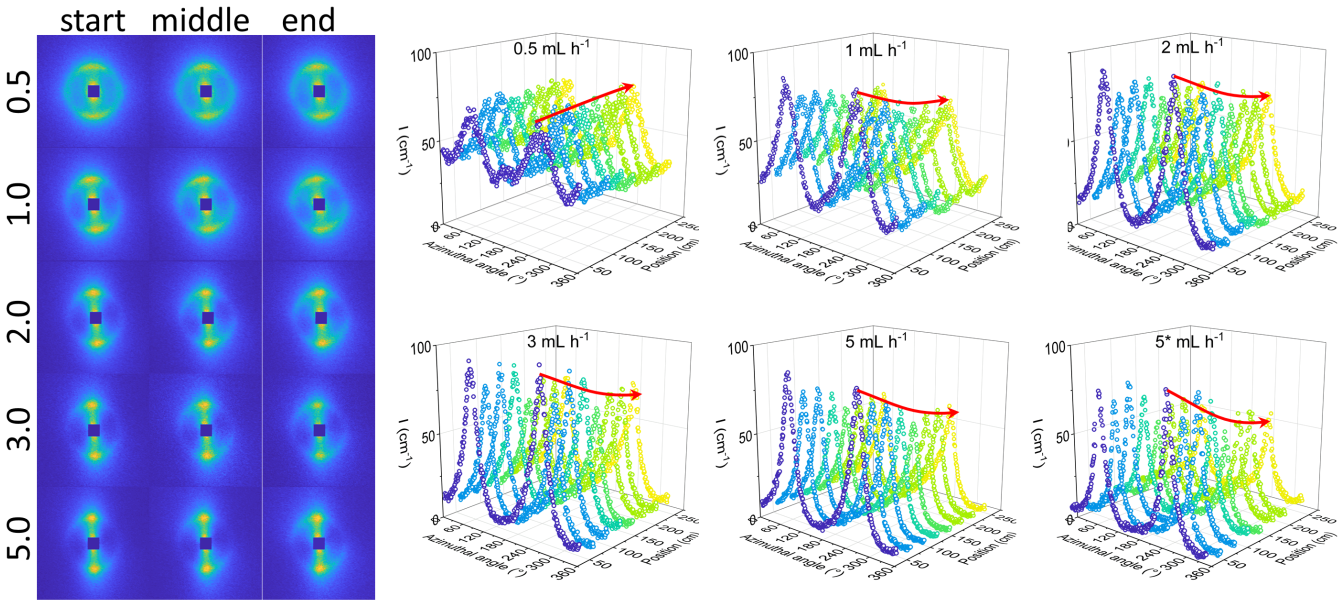

Figure S8: **2D SANS patterns acquired at three representative channel positions** (15, 130 and 245 cm, termed ‘start’, ‘middle’, ‘end’) at selected flow rates 0.5, 1.0, 2.0, 3.0 and 5.0 mL h^{-1} indicated. Azimuthal profile evolution along the channel at the respective 5 distinct flow rates, as well after cessation of flow at 5.0 mL h^{-1}, indicated as 5* mL h^{-1}. A subset of these data is presented in Fig. 8c of the main paper.

6 Comparison between serpentine microchannel flow experiments at 2% NaCl and previous oscillatory microflow data [1].

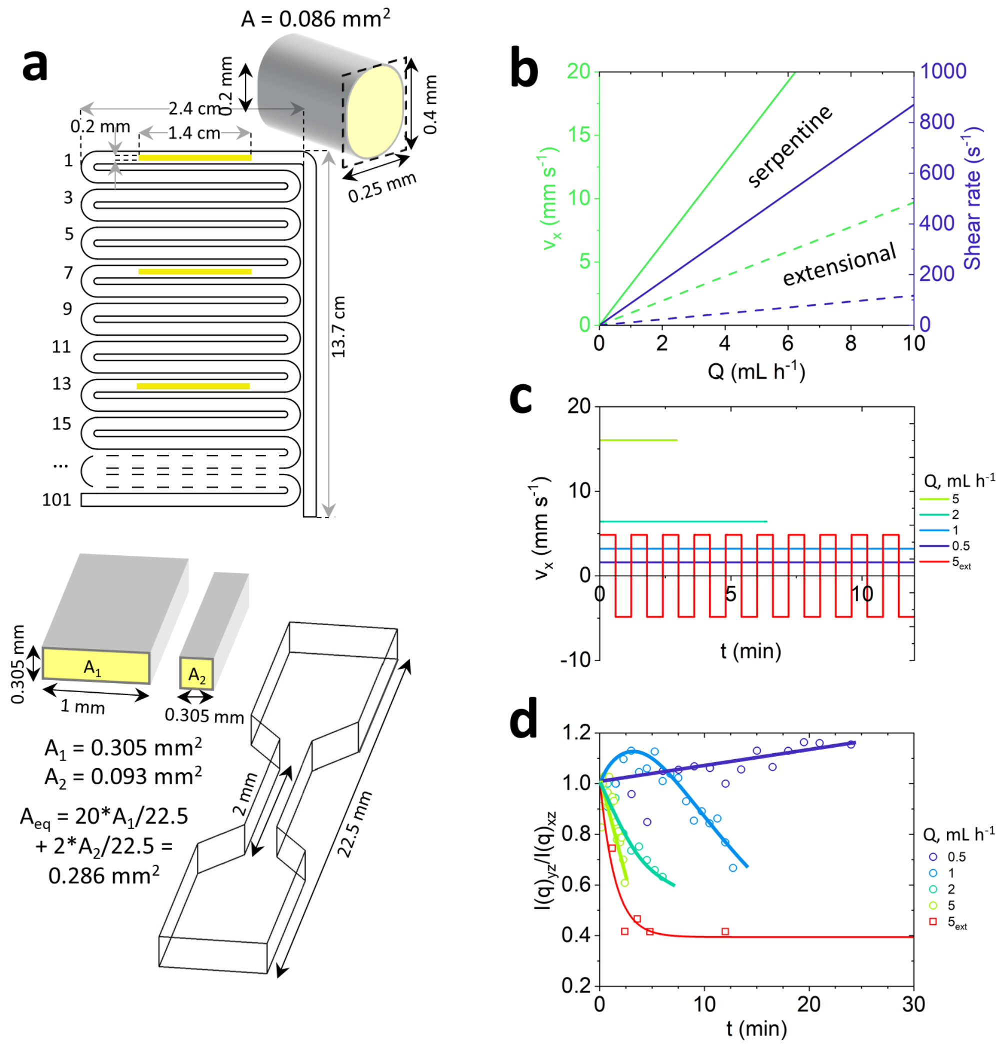

Figure S9: **Comparison of the flow effects induced by serpentine and extensional/oscillatory microfluidic chip geometries**. a) Microdevice geometry and channel cross-sections, including cros-sectional areas; b) Average linear velocity v_x and wall shear rate estimates as a function of volumetric flow rates; c) Imposed average flow velocity as the corresponding volumetric flow rates: horizontal lines correspond to the serpentine channel (0.5, 1.0, 2.0 and 5.0 mL h^{-1}), while the square wave indicates the velocity (wide cross-section) within the extensional/oscillatory field at 5 mL h^{-1}; d) Normalised $I(q)_{yz}/I(q)_{xz}$ evolution comparison between extensional geometry at 5 mL h^{-1} and linear serpentine geometry at 0.5, 1.0, 2.0 and 5.0 mL h^{-1}.

References

[1] L. Donina, A. Rafique, S. Khodaparast, L. Porcar, and J. T. Cabral, *Soft Matter* 2021, **17**, 44, 10053–10062.